The representation of marine surface fluxes is linked to intertropical convergence zone biases

Charlotte A. DeMott[1], **Carol Anne Clayson**[2], **Mark D. Branson**[1], **Jeremiah Brown**[2], **Chia-Wei Hsu**[3]

[1]Department of Atmospheric Science, Colorado State University, Fort Collins, Colorado
[2]Woods Hole Oceanographic Institution, Massachusetts
[3]NOAA PSL, Boulder, Colorado

Key Points:

- We compute model flux biases relative to those that would have resulted with the state-of-the-art COARE bulk flux algorithm
- Compared to COARE fluxes, twelve of fourteen CMIP6 models overestimate fluxes in the Intertropical Convergence Zone (ITCZ) region
- Replacing the default flux algorithm with the COARE algorithm in two global models reduces the double ITCZ bias

---

Corresponding author: Charlotte A. DeMott, `Charlotte.DeMott@Colostate.edu`

Abstract

Ocean-atmosphere coupled climate models struggle to produce a single northern hemisphere intertropical convergence zone (ITCZ), and instead simulate ITCZ bands in both hemispheres. This “double ITCZ” bias can negatively impact representations of large-scale modes of variability, such as the Madden-Julian oscillation and El Niño–Southern Oscillation. A new method to estimate model fluxes that would have been obtained with the COARE3.0 bulk flux algorithm indicates that twelve of fourteen CMIP6 models overestimate surface fluxes in the ITCZ region, suggesting that biases rooted in model flux algorithms may contribute to ITCZ biases. This finding is supported by atmosphere-only simulations of two models where the original flux algorithms are replaced with the COARE3.0 algorithm. In the experiments, precipitation root mean square errors in the double ITCZ region were reduced by 26% and 15%, respectively. We interpret these findings through the lenses of global energy constraints and convection-boundary layer interactions.

Plain Language Summary

Models used to study Earth’s present and future climates often struggle to reproduce the correct patterns of mean rainfall over the tropical oceans. When averaged over time and across all longitudes, models tend to produce two tropical rainfall peaks on either side of the Equator, whereas only a single peak just north of the Equator is observed in the real world. In this study, we show that the methods used to estimate the transfer of energy in and out of the ocean may be one reason for why models have difficulty with their representations of mean rainfall in the tropics.

1 Introduction

The intertropical convergence zone (ITCZ) is a zonally oriented band of enhanced cloudiness and rainfall observed over most of the globe. The latitude of ITCZ precipitation migrates seasonally, both in a global sense, and within each ocean basin (Donohoe et al., 2013; Koutavas & Lynch-Stieglitz, 2004; Richter et al., 2017; Sikka & Gadgil, 1980; Wei & Bordoni, 2018). The ITCZ acts as a waveguide for tropical convective disturbances (Ferreira & Schubert, 1997; Gonzalez et al., 2017) and helps maintain ocean circulations that sustain biological activity and promote ocean CO_2 uptake (Xie & Philander, 1994; Kessler, 2006).

Global climate models that form the basis of the Intergovernmental Panel on Climate Change (IPCC) assessment reports (on Climate Change (IPCC), 2023) have long struggled to simulate the observed single, northern hemisphere ITCZ, and instead exhibit strong preferences for double ITCZs (Fiedler et al., 2020). The double ITCZ bias has been implicated in the misrepresentation of large-scale modes of tropical climate variability, such as the Madden-Julian oscillation (Jiang et al., 2020) and El Niño–Southern Oscillation (ENSO; Guilyardi et al. (2003); Wittenberg et al. (2006)). Its interference with the simulation of these modes contributes to uncertainty in predicted changes to tropical-extratropical teleconnection patterns with rising CO_2 concentrations (e.g., Henderson et al. (2017); J. Wang et al. (2022)).

Identifying the root causes of the double ITCZ bias has challenged the climate community for decades. Models that simulate a double ITCZ in the eastern Pacific also tend to simulate excessively strong and westward-extended equatorial cold tongues (Lin, 2007; Samanta et al., 2019). These biases may be linked through an excessive Bjerknes feedback (Lin, 2007; Li & Xie, 2014) that intensifies the cold tongue bias, SST gradient-driven boundary layer convergence (Lindzen & Nigam, 1987; Back & Bretherton, 2009) that favors the maintenance of convection on both sides of the Equator, or a too-positive feedback of sea surface temperatures (SSTs) to surface fluxes and convective initiation (C. Zhang, 2001). Other studies indicate that biases in the sensitivity of convection to free tropospheric moisture contribute to weakening of subtropical subsidence on both sides of the Equator, thus favoring the formation of the southern ITCZ (Song & Zhang, 2018).

ITCZ location (i.e., its mean latitude) can also be thought of as a response to interhemispheric imbalances in the atmospheric heating, which drives the vertically integrated and zonally averaged cross-equator atmospheric energy transport (AET) (Neelin & Held, 1987; Hwang & Frierson, 2013). With this paradigm, the ITCZ location is shifted toward the hemisphere with more net heating and the resulting asymmetric Hadley circulation transports heat to the hemisphere with less net heating (Bischoff & Schneider, 2014, 2016), as shown in the upper panel of Figure 1a. The net heating in both southern and northern hemispheres set the interhemispheric imbalance and ITCZ asymmetry. This implies that biases far removed from the tropics, such as the albedo of Southern Ocean clouds (Hwang & Frierson, 2013) or heat uptake by the Atlantic meridional overturning circulation (C. Wang et al., 2014; S. Yu & Pritchard, 2019), can affect the interhemispheric heating contrast, and thus the AET, and contribute to the double ITCZ bias by erroneously shifting the ITCZ to the Southern Hemisphere (Adam, Schneider, et al., 2016).

Recent theoretical work based on the global energy budget suggests that the sensitivity of ITCZ meridional position to interhemispheric heating imbalances is modulated by the meridional structure of the net atmospheric energy input (AEI) about the Equator (Bischoff & Schneider, 2016). AEI, which is sometimes also referred to as “net energy input” (NEI), is defined as $AEI = \mathcal{S} - \mathcal{L} - \mathcal{O}$ where $\mathcal{S}$ and $\mathcal{L}$ are respectively net atmospheric heating by shortwave and longwave radiation, and $\mathcal{O}$ is the net ocean heat uptake. Bischoff and Schneider (2016) showed that the meridional curvature of zonally averaged AEI about the Equator affects the sensitivity of the ITCZ position to AET, as illustrated in Figure 1a–c. In particular, when AEI is small compared to the interhemispheric heating imbalance-driven AET, the ITCZ shifts farther into the warm hemisphere (Figure 1a). When AEI minimizes near the Equator, as observed on Earth, the curvature effect reduces the sensitivity of ITCZ position to AET, and the ITCZ shifts southward (Figure 1b), or bifucates into a double ITCZ for negative AEI (Figure 1c).

The above examples illustrate how ITCZ position is sensitive to subtle changes in AEI near the Equator and provides a framework for understanding how AET and equatorial AEI together control ITCZ position on Earth (Adam, Bischoff, & Schneider, 2016) and in models (Adam, Schneider, et al., 2016; Wei & Bordoni, 2018). It can be leveraged to interpret changes to simulated ITCZ states that arise with changes to model settings such as e.g., turbulence and cumulus parameterization (Hagos et al., 2021; Lu et al., 2021; Talib et al., 2018; Song & Zhang, 2018) or ocean coupling (Talib et al., 2020; Lee et al., 2022). Many of these and other studies have identified clouds and their radiative feedbacks (Woelfle et al., 2019; G. J. Zhang et al., 2019) and ocean circulations (Green & Marshall, 2017) as being responsible for biases in both interhemispheric energy imbalances and equatorial AEI that affect ITCZ biases. In contrast, less attention has focused on marine surface latent heat fluxes and their biases as a source of ITCZ bias in climate models.

Zonally averaged mean surface latent heat fluxes, which dominate the ocean-atmosphere energy exchange, differ by as much as 50 W m^{-2} in the tropics (R. Zhang et al., 2018) and up to 18 W m^{-2} in the global mean (Wild et al., 2015; Wild, 2020) for models participating in the IPCC Coupled Model Intercomparison Projects 5 and 6 (CMIP5 and CMIP6; Taylor et al. (2012); Eyring et al. (2016)). In models, fluxes are computed with bulk surface flux algorithms that estimate the flux based on the simulated surface temperature and low-level wind speed, temperature, and humidity (i.e., the “bulk” inputs):

$$LH = \rho C_e L_v U_{10} \Delta q \tag{1}$$

where ρ is the density of water, C_e is the bulk transfer coefficient, L_v is the latent heat of vaporization, U_{10} is wind speed, adjusted to 10 m, and $\Delta q = 0.98 q^*_{SST} - q_{2m}$ where

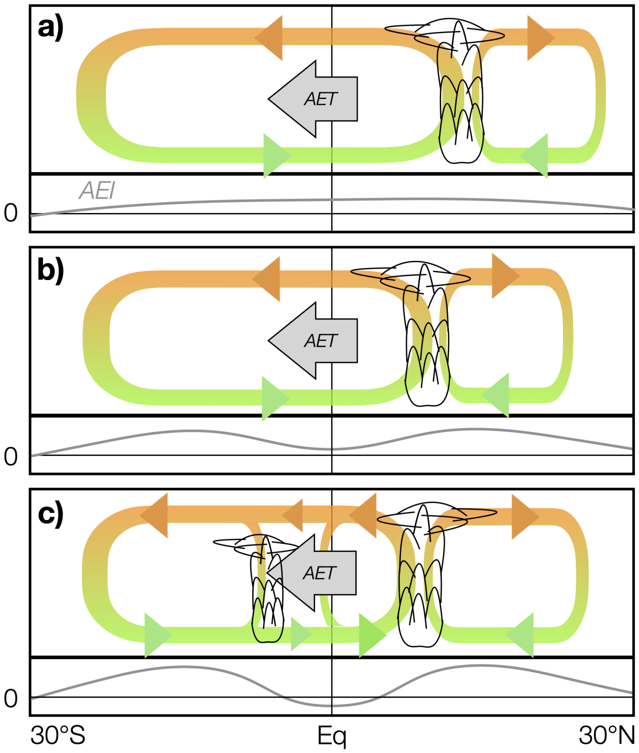

Figure 1. Schematic illustration of the relationship between ITCZ location and atmospheric energy input (AEI; gray lines in each lower panel) for a given cross-equatorial atmospheric energy transport (AET; gray arrows) as described in Bischoff and Schneider (2016). AET is the same in a–c, but ITCZ position, denoted by clouds, varies with the meridional distribution of AEI. The mean meridional moisture and energy transports are shown with green and orange arrows, respectively. Note that AEI curvature about the Equator increases from a–c.

q^*_{SST} and q_{2m} are saturation specific humidity at SST and specific humidity at 2 m, respectively, and the 0.98 factor applied to q^*_{SST} accounts for the reduction in saturation specific humidity by ocean salinity effects (Zeng et al., 1998). Biases in surface fluxes can therefore be rooted in biases in any of the bulk inputs, as well as in the algorithm used to estimate the bulk transfer coefficient, C_e (L. Yu, 2019).

It has been shown that different bulk flux algorithms can yield a wide range of fluxes given the same bulk inputs, and that the majority of flux algorithms appearing in the literature overestimate marine surface fluxes by 10–20% when compared to fluxes computed from direct covariance measurements (Brunke et al., 2003). These differences, which are rooted in the assumptions and methods used to empirically relate the bulk inputs to the flux, are most evident at high and low wind speeds (Brodeau et al., 2017), and are thus not uniformly distributed across the range of bulk input variables. Of the twelve bulk flux algorithms analyzed by Brunke et al. (2003), the COARE3.0 algorithm (Fairall, Bradley, Rogers, et al., 1996; Fairall et al., 2003) was judged to be one of the least problematic when compared to in situ direct covariance-measured fluxes at several locations across the globe. The COARE3.0 algorithm (hereafter, simply referred to as "COARE") is used to compute surface latent and sensible heat fluxes from in situ surface meteorology measured at tropical moorings (McPhaden et al., 2010)and is the basis of all modern satellite-derived surface flux products (L. Yu, 2019). In contrast, surface fluxes in climate models are computed using a multitude of bulk flux algorithms (Brodeau et al., 2017), some of which include adjustments to account for flux dependence on low-level stability, subgridscale gustiness, or other factors (Zeng et al., 1998; Harrop et al., 2018).

In this study, we present evidence to suggest that biases in climate models' bulk flux formulae favors tropical AEI distributions that exacerbate the double ITCZ bias in those models. Replacing the original bulk flux algorithm with the COARE algorithm in atmosphere-only simulations of two climate models flattens their meridional AEI gradients and reduces their double ITCZ biases in a manner consistent with the results of Bischoff and Schneider (2016). These changes to mean eastern tropical Pacific precipitation are considered through the lens of marine boundary layer-convection interactions.

Our study is outlined as follows: Datasets and diagnostic methods are described in Section 2. Model flux biases are described in Section 3. In Section 4, we test the sensitivity of ITCZ structure to bulk flux algorithm in two global models by replacing the native flux algorithm with the COARE algorithm. Conclusions are given in Section 5.

2 Methods and Data

2.1 Data

We analyze surface latent heat fluxes in historical simulations of models participating in the International Panel on Climate Change 6th Assessment Report Coupled Model Intercomparison Project (CMIP6; Eyring et al. (2016)). Daily mean values of 10 m wind speed (U_{10}; m s^{-1}), 2 m specific humidity (q_{2m}; g kg^{-1}), SST (K) (i.e., temperature of the top-most layer of the ocean model) and LH (W m^{-2}) are used to diagnose model fluxes as a function of bulk inputs, while daily mean 2 m air temperature ($T_{2m}; K$) is used to assess stability of the marine atmospheric boundary layer. Fourteen modeling centers (Table **??**) provided these inputs at daily resolution, and we analyzed only the first available ensemble member (usually *r1i1p1f1*) for simulation years 1995-2014.

Model output is compared to in situ observations of U_{10}, q_{2m}, and SST measured by moorings throughout the global tropics (30°N–30°S) and made available through the Global Tropical Moored Buoy Array (McPhaden et al., 2010). Sampling period, data quality, and data continuity vary widely from mooring to mooring. Since our analysis does not require a continuous data stream, we only analyze "highest quality" observations of U_{10}, q_{2m}, and SST (i.e., data quality code 1). Simulated precipitation climatologies are compared to the Integrated Multi-satellitE Retrievals for GPM from June 2000–May 2019 (IMERG; Huffman et al. (2020)). All model and observational fields are interpolated to a 2.5×2.5 latitude-longitude grid prior to diagnosing the flux.

2.2 Diagnosis of surface fluxes

In this study, we do not compute surface fluxes, but diagnose their daily mean values as a function of their daily mean bulk inputs. U_{10} is directly reported for both moorings and models, but Δq must be calculated starting from q_{2m} and SST. While SST used for bulk estimation of the flux refers to the ocean skin temperature (the temperature of the uppermost few microns of the ocean surface), SST measured by moorings corresponds to ocean temperatures at depths of ∼1 m while that reported by models equates to the mean ocean temperature of the uppermost model layer, which is typically $\mathcal{O}(10\text{ m})$.

Ocean temperature at depths 1 m or greater may vary substantially from ocean skin temperature owing to diurnal warming of the surface layer ($\mathcal{O}(1\text{ m})$) and molecular thermal cooling of the surface skin (Fairall, Bradley, Rogers, et al., 1996; Kawai & Wada, 2007). When averaged over the course of a day, the diurnal warm layer and “cool skin” effects partially offset each other, but the cool skin effect, which is not diurnally dependent, slightly dominates, yielding a daily mean skin temperature approximately 0.2 K cooler than the 1 m daily mean temperature measured by moorings (Donlon et al., 2007; Minnett & Kaiser-Weiss, 2012)). Hence, daily mean SST from moorings is reduced by 0.2 K before computing q^*_{SST}. We apply the same correction to model SST, although it is not always clear if diurnal warm layer and/or cool skin approximations have been applied before computing the flux. Fairall, Bradley, Godfrey, et al. (1996) (their Table 5) indicate that the combined effect of omitting these two SST corrections can inflate the mean LH by about 5%, or 5 W m^{-2}. However, as we show in the next section, this uncertainty is generally less than the flux difference arising from choice of bulk flux algorithm.

3 Comparison of CMIP6 surface fluxes to COARE surface fluxes

3.1 Diagnosis of model surface flux biases

Fluxes and their bulk inputs from all available mooring observations are aggregated into a single diagnostic by computing the mean flux as a function of U_{10} and Δq, as shown in Figure 2a. The relative frequency of U_{10}–Δq pairs is shown with contours, while the average flux per U_{10}–Δq bin—a function of the bulk transfer coefficient—is shaded. Consistent with Eq. 1, the flux increases with increasing U_{10} and Δq.

The single “grand flux matrix” in Figure 2a, which pools fluxes from across the global tropics, might mask changes to the flux that could arise from changes in SST, SST gradients, or low-level stability. To understand how these differences could affect the observed flux diagnostic, we computed a separate flux matrix for each mooring (FIGURE S1) and used the differences between individual flux matrices and the grand flux matrix in Figure 2a to compute the root mean square difference (RMSD). Figure 2b reveals that the magnitude of the bin-sampled flux varies little with geographic location. The largest absolute RMSDs, which amount to <5% differences, are observed infrequently, near the maximum and minimum values of U_{10} and Δq. We further investigate the dependence of the flux on low-level stability by computing the flux difference for unstable and stable boundary layers, as evaluated by the sign of the near-surface vertical temperature gradient, $\Delta T = SST - T_{2m}$, shown in Figure 2c. These differences are also small for the majority of U_{10}–Δq bins. These results demonstrate that the differences in surface fluxes by region or by stability regime are generally small compared to the mean flux. We therefore use the result shown in Figure 2a as the basis for our assessment of tropical flux biases in climate models.

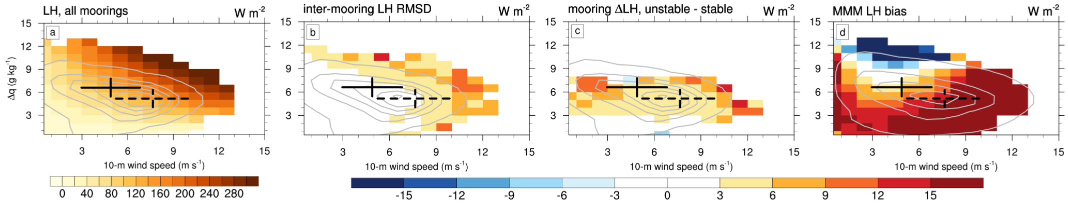

Figure 2. a) Surface fluxes compiled from all 30°S–30°N moorings; b) the flux root mean square difference between fluxes at an individual mooring and the composite result in a); c) mean flux difference for stable minus unstable boundary layer (i.e., where $\Delta T > 0$ or $\Delta T < 0$; $\Delta T = SST - T_{2m}$), d) the multi-model mean surface flux bias for the tropical oceans (ocean points from 30°S–30°N and 0°E–360°E). The frequency of wind speed-Δq input pairs is contoured (interval 1%). Solid and dashed crosses respectively mark the mean ±1 standard deviation of wind speed and Δq for the equatorial western Pacific and subtropical eastern Pacific regions shown in Figure 4.

The multi-model mean (MMM) tropical (30°S–30°N; 0°E–°360E) marine flux bias for historical simulations of fourteen CMIP6 models is shown in Figure 2d. In contrast to small observed flux differences that arise from mooring location or low-level stability, flux biases arising from model flux algorithms can be quite large. In general, models tend to overestimate the flux for lower values of Δq and with increasing values of U_{10}. The mean flux matrix and flux bias for individual models at a point collocated with the 165°E, 0°N mooring can be seen in Figures S1 and S2. Following (BONY 2004), we decomposed the flux bias into its contributions from input biases and algorithm biases (Figure S3), which demonstrated that, for most models, biases arising from the choice of bulk flux algorithm are as significant as those arising from biases in the bulk inputs. Thus, model surface flux biases arising from the choice of bulk flux algorithm cannot be ignored when assessing model fluxes.

The bin-by-bin ratio of the mooring-derived flux in Figure 2a to individual model flux can be leveraged to adjust the model flux to the COARE flux (Hsu et al., 2022). This offline correction yields a hypothetical flux timeseries for each model had the model-simulated U_{10} and Δq been input to the COARE flux algorithm, rather the model's native flux algorithm. We use this method to generate COARE-estimated fluxes for each model, and show a map of the multi-model mean flux difference in Figure 3.

Consistent with the findings of Brunke et al. (2003) and the result shown in Figure 2d, the flux correction reduces the flux throughout the tropics (Figure 3a). Flux corrections are larger in the subtropics than the tropics, with the largest corrections located upstream of precipitaiton biases, as inferred from low-level wind vectors in Figure 3a. The relative magnitude of the flux correction can be seen more clearly in Figure 3b which shows the same result after subtracting the MMM domain average correction. The large-scale pattern of the flux adjustment is robust across models, as indicated by stippling that denotes where the sign of the relative flux correction for each individual model agrees with that of the multi-model mean for at least twelve of the fourteen models (i.e., ≥86%). These results suggest that the COARE algorithm has the potential to reduce subtropical surface fluxes, and perhaps precipitation, in a region of persistent double ITCZ bias.

4 Simulated ITCZ with the COARE algorithm

The above analysis suggests that differences in model surface flux algorithms and the COARE flux algorithm may contribute to AEI and precipitation biases associated

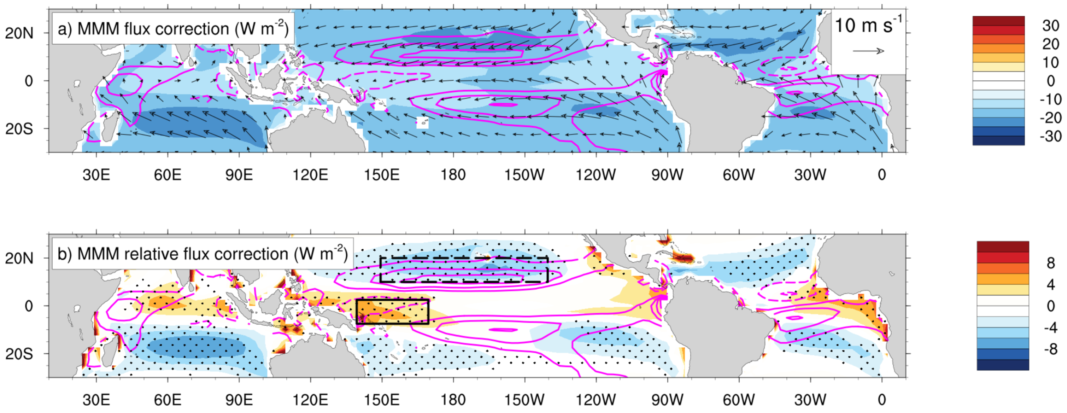

Figure 3. a) Multi-model mean (MMM) surface latent flux correction (W m^{-2}; shading) when adjusting model fluxes to COARE fluxes (see text and Hsu et al. (2022) for description of method), MMM 1000 hPa mean winds (vectors), and MMM precipitation bias relative to IMERG June 2000–May 2019 climatology (contours; interval 1 mm day^{-1}). b) MMM relative flux correction (shading) obtained by subtracting the domain-mean flux correction shown in a). Stippling indicates regions where the sign of the relative correction calculated for each model agrees with the sign of the MMM correction. Magenta contours as in a), and black dashed and solid rectangles indicate regions used to calculate standard deviations of U_{10} and Δq from moorings shown in Figure 2.

with the double ITCZ bias in climate models. To test this idea, we analyzed changes to surface fluxes, AEI, and precipitation in two atmosphere-only climate model simulations where the default flux algorithm in each model was replaced with the COARE flux algorithm. Atmosphere-only simulations were chosen to avoid changes to the flux and AEI driven by SST and ocean heat uptake differences. For the first model, the Department of Energy (DOE) Energy Exascale Earth System Model (E3SM; Golaz et al. (2019)), we analyze results provided by Eyre et al. (2021), who integrated the model for six years using a repeating cycle of SSTs from the year 2000. The same COARE flux code from the E3SM simulation was ported into the National Center for Atmospheric Research (NCAR) Community Earth System Model, version 2 (CESM2; Danabasoglu et al. (2020)) to perform a 36 year simulation forced with observed SSTs from 1979–2014. The E3SM and CESM2 share a common lineage, and both compute surface flux bulk transfer coefficients according to Large and Yeager (2004) (hereafter LY) in their default configurations. Compared to the LY algorithm, the COARE algorithm uses three stability classes rather than two, computes roughness length as a continuously varying function of wind speed rather than as a constant value for each stability class, and includes a gustiness factor to better represent fluxes in low wind conditions.

The zonally averaged AEI over oceans for both models and their differences for each flux experiment are shown in Figure 4a–c. Compared to the LY flux algorithm, the COARE algorithm in both models changes the sign of equatorial AEI from weakly negative to weakly positive in better agreement with observations (Bischoff & Schneider, 2016), and decreases subtropical AEI (Figures 4b, c). For both models, the meridional structure of AEI changes bears a strong resemblance to the meridional structure of *LH* changes (Figure 4b), suggesting a strong connection between the two.

Mean rainfall and its changes with the COARE algorithm are shown in Figure 4d–f. The models differ from IMERG climatology in two notable ways. First, they produce less rainfall on the Equator and, second, the meridional widths of their northern and southern precipitation maxima are too broad (Figure 4d and dashed lines in Figure 4e). Replacing the LY flux algorithm with the COARE algorithm reduces both of these biases in each model (solid lines in Figure 4d and Figure 4e).

The changes to AEI and precipitation with COARE fluxes are partly consistent with theoretically determined constraints on ITCZ position arising from hemispheric asymmetries in AEI (Bischoff & Schneider, 2016). In particular, a change in sign of AEI at the Equator from negative to positive has been associated with a shift away from a double ITCZ toward a single ITCZ in the Northern Hemisphere (e.g., Figure 1b, c). Although the COARE algorithm increases AEI and rainfall on the Equator, a weak double ITCZ structure remains. That the weakly double ITCZ structure is seen in both IMERG observations and in experiments with the COARE flux algorithm may reflect influences of other processes, including local effects, in determining ITCZ structure.

We interpret changes to ITCZ width with the COARE algorithm through the lens of boundary layer buoyancy-convection interactions. Marine boundary layer buoyancy is regulated by fluxes of heat and moisture from the ocean surface, inputs of free tropospheric air across the boundary layer top by entrainment and convectively driven downdrafts, and horizontal advection of temperature and moisture (de Szoeke et al., 2017), as well as mass convergence driven by cold pools and SST gradients (Zuidema et al., 2012; Back & Bretherton, 2009). Wolding et al. (2022) have shown that the initiation and development of tropical convection is jointly regulated by the buildup of buoyancy in the boundary layer and the relative dilution of buoyancy in the lower free troposphere. A reduction in boundary layer buoyancy, or a delay in its increase following an air mass trajectory would therefore delay the onset of convection. Hence, we attribute COARE algorithm-induced precipitation reductions on the poleward flank of each ITCZ band (Figure 4e) to the large subtropical surface flux reductions that occur upstream of precipitation biases in each basin (Figure 3a).

This line of reasoning is consistent with theoretically determined controls of ITCZ width based on energetic constraints by Byrne and Schneider (2016), who argued that ITCZ width should be sensitive to the tropical AEI, the advection of moist static energy by the Hadley circulation and by transient eddies, and the gross moist stability. The relationship of surface flux changes to the first two of these controls (AEI and advection of moist static energy) has been shown or inferred herein, while understanding the effects of bulk flux algorithm on the latter two (transient eddies and gross moist stability) will require further analysis. Our findings are also consistent the ITCZ energetics analysis of CMIP5 models by Adam, Schneider, et al. (2016) ADAMS ET AL 2016, who found that tropical surface energy fluxes were not related to the spread in the asymmetric aspects of the double-ITCZ bias in climate models, but were instead related to biases in tropical AEI, particularly the negative bias near the Equator.

5 Conclusions

Marine surface fluxes are an essential component of the Earth's water and energy cycles, yet they remain poorly constrained owning to a relative lack of in situ observations (Clayson et al., 2023). In climate models, a lack of consistent methods for estimating surface fluxes contributes to uncertainties in their role in shaping mean cloudiness patterns that influence the mean state climate.

This study leverages surface flux diagnostics, theoretical advances in understanding mean ITCZ structure, and model experiments to demonstrate that the choice of bulk flux algorithm in climate models can lead to surface flux biases which contribute to pervasive ITCZ biases in climate models (e.g., Fiedler et al. (2020)). In atmosphere-ocean coupled models, these biases are often attributed to the excessive cold tongue bias in the equatorial eastern Pacific. Our experiments, which utilize atmosphere-only simulations

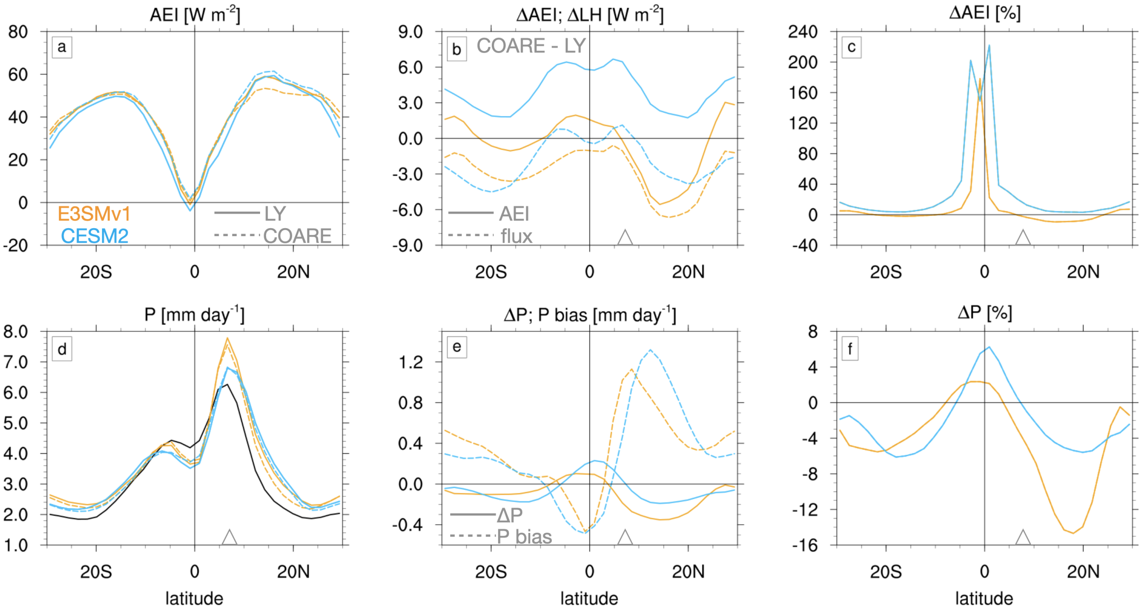

Figure 4. 30°N–30°S zonally averaged atmospheric energy input (AEI; top row) and precipitation (bottom row) for E3SMv1 (orange) and CESM2 (cyan) atmosphere-only simulations. a) AEI by latitude for LY (solid) and COARE (dashed) fluxes; b) COARE minus LY difference (Δ) in AEI (solid) and LH (dashed); c) AEI percent change (ΔAEI / $|\mathrm{AEI}_{LY}|$); d) mean precipitation for IMERG (black) and for LY and COARE simulations; e) precipitation change (solid) and precipitation bias (dashed) for LY simlations; f) precipitation percent change. Triangles at 7°N in b–f mark location of maximum mean precipitation for regridded IMERG observations and simulations.

forced with observed SSTs, reveal that ITCZ biases can also be rooted in methods used to estimate ocean-to-atmosphere surface fluxes, even in the absence of SST biases.

In our study, surface fluxes estimated using the COARE bluk flux algorithm are treated as "truth." This algorithm, which is one of the least biased when compared to in situ surface flux observations (Brunke et al., 2003) is nevertheless subject to uncertainties common to many algorithms. To reduce these uncertainties, more observations are needed to better characterize surface fluxes in high wind conditions, across atmospheric stability regimes, in the vicinity of sharp SST gradients, and under a variety of sea states (i.e., wave conditions). As climate models incorporate these advances in their surface flux parameterizations, reductions in long-standing biases such as the double ITCZ and the eastern Pacific cold tongue may be reduced, thus building confidence in models' abilities to simulate the current and future climate.

6 Open Research

Tropical mooring data are available from the Global Tropical Moored Buoy Array at `https://www.pmel.noaa.gov/tao/drupal/disdel/`.

CMIP6 multi-model ensemble data analyzed as part of this project were downloaded from the Earth System Grid Federation at `https://esgf-node.llnl.gov/projects/cmip6/`. Monthly mean IMERG rainfall data (HUFFMAN ET AL 2023) are available from `https://disc.gsfc.nasa.gov/datacollection/GPM_3IMERGM_07.html`.

Python code used to compute the surface latent heat flux diagnostics shown in Figure 2 is available through the NOAA Model Diagnsotics Task Force Diagnostics Package at `https://www.gfdl.noaa.gov/mdtf-diagnostics/`.

Acknowledgments

CAD and CWH were supported by the Department of Energy Biological and Environmental Research Program (DE-SC0020324). CAD, CAC, MB, and JB received support from NOAA Modeling, Analysis, Predictions and Projections (MAPP; NA20OAR4310389).

We acknowledge the World Climate Research Programme, which, through its Working Group on Coupled Modelling, coordinated and promoted CMIP6. We thank the climate modeling groups for producing and making available their model output, the Earth System Grid Federation (ESGF) for archiving the data and providing access, and the multiple funding agencies who support CMIP6 and ESGF.

References

Adam, O., Bischoff, T., & Schneider, T. (2016). Seasonal and interannual variations of the energy flux equator and itcz. part i: Zonally averaged itcz position. *Journal of Climate*, *29*(9), 3219–3230.

Adam, O., Schneider, T., Brient, F., & Bischoff, T. (2016). Relation of the double-ITCZ bias to the atmospheric energy budget in climate models. *Geophysical Research Letters*, *43*(14), 7670–7677.

Back, L. E., & Bretherton, C. S. (2009, aug). On the relationship between SST gradients, boundary layer winds, and convergence over the tropical oceans. *J. Climate*, *22*(15), 4182–4196.

Bischoff, T., & Schneider, T. (2014). Energetic constraints on the position of the intertropical convergence zone. *Journal of Climate*, *27*(13), 4937–4951.

Bischoff, T., & Schneider, T. (2016). The equatorial energy balance, ITCZ position, and double-ITCZ bifurcations. *Journal of Climate*, *29*(8), 2997–3013.

Brodeau, L., Barnier, B., Gulev, S. K., & Woods, C. (2017, jan). Climatologically significant effects of some approximations in the bulk parameterizations of turbulent air–sea fluxes. *Journal of Physical Oceanography*, *47*(1), 5–28. doi: 10.1175/jpo-d-16-0169.1

Brunke, M. A., Fairall, C. W., Zeng, X., Eymard, L., & Curry, J. A. (2003). Which bulk aerodynamic algorithms are least problematic in computing ocean surface turbulent fluxes? *Journal of Climate*, *16*(4), 619–635.

Byrne, M. P., & Schneider, T. (2016, jun). Energetic constraints on the width of the intertropical convergence zone. *Journal of Climate*, *29*(13), 4709–4721. doi: 10.1175/jcli-d-15-0767.1

Clayson, C. A., DeMott, C. A., de Szoeke, S. P., Chang, P., Foltz, G. R., Krishnamurthy, R., ... Zuidema, P. (2023). *A new paradigm for observing and modeling of air-sea interactions to advance earth system prediction* (Tech. Rep.). doi: 10.5065/24J7-W583

Danabasoglu, G., Lamarque, J.-F., Bacmeister, J., Bailey, D. A., DuVivier, A. K., Edwards, J., ... Strand, W. G. (2020, feb). The community earth system model version 2 (CESM2). *Journal of Advances in Modeling Earth Systems*, *12*(2). doi: 10.1029/2019ms001916

de Szoeke, S. P., Skyllingstad, E. D., Zuidema, P., & Chandra, A. S. (2017, apr). Cold pools and their influence on the tropical marine boundary layer. *Journal of the Atmospheric Sciences*, *74*(4), 1149–1168. doi: 10.1175/jas-d-16-0264.1

Donlon, C., Robinson, I., Casey, K., Vazquez-Cuervo, J., Armstrong, E., Arino, O., ... others (2007). The global ocean data assimilation experiment high-resolution sea surface temperature pilot project. *Bulletin of the American Meteorological Society*, *88*(8), 1197–1214.

Donohoe, A., Marshall, J., Ferreira, D., & Mcgee, D. (2013). The relationship between ITCZ location and cross-equatorial atmospheric heat transport: From the seasonal cycle to the Last Glacial Maximum. *Journal of Climate*, *26*(11), 3597–3618.

Eyre, J. E. J. R., Zeng, X., & Zhang, K. (2021, may). Ocean surface flux algorithm effects on earth system model energy and water cycles. *Frontiers in Marine Science*, *8*. doi: 10.3389/fmars.2021.642804

Eyring, V., Bony, S., Meehl, G. A., Senior, C. A., Stevens, B., Stouffer, R. J., & Taylor, K. E. (2016). Overview of the coupled model intercomparison project phase 6 (CMIP6) experimental design and organization. *Geosci. Model Dev.*, *9*, 1937–1958.

Fairall, C. W., Bradley, E. F., Godfrey, J. S., Wick, G. A., Edson, J. B., & Young, G. S. (1996, jan). Cool-skin and warm-layer effects on sea surface temperature. *Journal of Geophysical Research: Oceans*, *101*(C1), 1295–1308. doi: 10.1029/95jc03190

Fairall, C. W., Bradley, E. F., Hare, J. E., Grachev, A. A., & Edson, J. B. (2003). Bulk parameterization of air–sea fluxes: updates and verifications for the COARE algorithm. *J. Climate*, *16*.

Fairall, C. W., Bradley, E. F., Rogers, D. P., Edson, J. B., & Young, G. S. (1996). Bulk parameterization of air-sea fluxes for Tropical Ocean–Global Atmosphere Coupled–Ocean Atmosphere Response Experiment. *J. Geophys. Res.*, *101*(C2), 3747.

Ferreira, R. N., & Schubert, W. H. (1997). Barotropic aspects of ITCZ breakdown. *Journal of the Atmospheric Sciences*, *54*(2), 261–285.

Fiedler, S., Crueger, T., D'Agostino, R., Peters, K., Becker, T., Leutwyler, D., ... others (2020). Simulated tropical precipitation assessed across three major phases of the coupled model intercomparison project (cmip). *Monthly Weather Review*, *148*(9), 3653–3680.

Golaz, J.-C., Caldwell, P. M., Roekel, L. P. V., Petersen, M. R., Tang, Q., Wolfe, J. D., ... Zhu, Q. (2019, jul). The DOE e3sm coupled model version 1: Overview and evaluation at standard resolution. *Journal of Advances in Mod-*

eling Earth Systems, *11*(7), 2089–2129. doi: 10.1029/2018ms001603

Gonzalez, A. O., Mora Rojas, G., Schubert, W. H., & Taft, R. K. (2017). Transient aspects of the Hadley circulation forced by an idealized off-equatorial ITCZ. *Journal of Advances in Modeling Earth Systems*, *9*(1), 668–690.

Green, B., & Marshall, J. (2017). Coupling of trade winds with ocean circulation damps ITCZ shifts. *Journal of Climate*, *30*(12), 4395–4411.

Guilyardi, E., Delecluse, P., Gualdi, S., & Navarra, A. (2003). Mechanisms for enso phase change in a coupled gcm. *Journal of climate*, *16*(8), 1141–1158.

Hagos, S. M., Leung, L. R., Garuba, O. A., Demott, C., Harrop, B., Lu, J., & Ahn, M.-S. (2021). The relationship between precipitation and precipitable water in CMIP6 simulations and implications for tropical climatology and change. *Journal of Climate*, *34*(5), 1587–1600.

Harrop, B. E., Ma, P.-L., Rasch, P. J., Neale, R. B., & Hannay, C. (2018, apr). The role of convective gustiness in reducing seasonal precipitation biases in the tropical west Pacific. *Journal of Advances in Modeling Earth Systems*, *10*(4), 961–970. Retrieved from `https://doi.org/10.1002%2F2017ms001157` doi: 10.1002/2017ms001157

Henderson, S. A., Maloney, E. D., & Son, S.-W. (2017). Madden–Julian oscillation Pacific teleconnections: The impact of the basic state and mjo representation in general circulation models. *Journal of Climate*, *30*(12), 4567–4587.

Hsu, C.-W., DeMott, C. A., Branson, M. D., Eyre, J. R., & Zeng, X. (2022, apr). Ocean surface flux algorithm effects on tropical indo-pacific intraseasonal precipitation. *Geophysical Research Letters*, *49*(7). doi: 10.1029/2021gl096968

Huffman, G. J., Bolvin, D. T., Braithwaite, D., Hsu, K.-L., Joyce, R. J., Kidd, C., ... Xie, P. (2020). Integrated multi-satellite retrievals for the global precipitation measurement (GPM) mission (IMERG). In *Advances in global change research* (pp. 343–353). Springer International Publishing. doi: 10.1007/978-3-030-24568-9_19

Hwang, Y.-T., & Frierson, D. M. (2013). Link between the double-intertropical convergence zone problem and cloud biases over the Southern Ocean. *Proceedings of the National Academy of Sciences*, *110*(13), 4935–4940.

Jiang, X., Maloney, E., & Su, H. (2020). Large-scale controls of propagation of the Madden-Julian Oscillation. *NPJ Climate and Atmospheric Science*, *3*(1), 29.

Kawai, Y., & Wada, A. (2007). Diurnal sea surface temperature variation and its impact on the atmosphere and ocean: A review. *Journal of oceanography*, *63*, 721–744.

Kessler, W. S. (2006). The circulation of the eastern tropical pacific: A review. *Progress in Oceanography*, *69*(2-4), 181–217.

Koutavas, A., & Lynch-Stieglitz, J. (2004). Variability of the marine itcz over the eastern pacific during the past 30,000 years: Regional perspective and global context. In *The hadley circulation: Present, past and future* (pp. 347–369). Springer.

Large, W., & Yeager, S. (2004). *Diurnal to decadal global forcing for ocean and sea-ice models: The data sets and flux climatologies* (Tech. Rep.). doi: 10.5065/D6KK98Q6

Lee, J., Kang, S. M., Kim, H., & Xiang, B. (2022). Disentangling the effect of regional SST bias on the double-ITCZ problem. *Climate Dynamics*, *58*(11-12), 3441–3453.

Li, G., & Xie, S.-P. (2014). Tropical biases in CMIP5 multimodel ensemble: The excessive equatorial Pacific cold tongue and double ITCZ problems. *Journal of Climate*, *27*(4), 1765–1780.

Lin, J.-L. (2007). The double-ITCZ problem in IPCC AR4 coupled GCMs: Ocean–atmosphere feedback analysis. *Journal of Climate*, *20*(18), 4497–4525.

Lindzen, R. S., & Nigam, S. (1987). On the role of sea surface temperature gradients in forcing low-level winds and convergence in the tropics. *Journal of At-*

mospheric Sciences, *44*(17), 2418–2436.

Lu, Y., Wu, T., Li, Y., & Yang, B. (2021). Mitigation of the double ITCZ syndrome in BCC-CSM2-MR through improving parameterizations of boundary-layer turbulence and shallow convection. *Geoscientific Model Development*, *14*(8), 5183–5204.

McPhaden, M., McPhaden, M., McPhaden, M., McPhaden, M., McPhaden, M., McPhaden, M., … McPhaden, M. (2010, dec). The global tropical moored buoy array. In *Proceedings of OceanObs'09: Sustained ocean observations and information for society.* European Space Agency. doi: 10.5270/oceanobs09.cwp.61

Minnett, P., & Kaiser-Weiss, A. (2012). Near-surface oceanic temperature gradients. *GHRSST Discussion Doc*, *7*.

Neelin, J. D., & Held, I. M. (1987). Modeling tropical convergence based on the moist static energy budget. *Monthly Weather Review*, *115*(1), 3–12.

on Climate Change (IPCC), I. P. (2023). *Climate change 2022 – impacts, adaptation and vulnerability.* Cambridge University Press. doi: 10.1017/9781009325844

Richter, I., Xie, S.-P., Morioka, Y., Doi, T., Taguchi, B., & Behera, S. (2017). Phase locking of equatorial atlantic variability through the seasonal migration of the ITCZ. *Climate Dynamics*, *48*, 3615–3629.

Samanta, D., Karnauskas, K. B., & Goodkin, N. F. (2019). Tropical pacific SST and ITCZ biases in climate models: Double trouble for future rainfall projections? *Geophysical Research Letters*, *46*(4), 2242–2252.

Sikka, D., & Gadgil, S. (1980). On the maximum cloud zone and the ITCZ over indian longitudes during the southwest monsoon. *Monthly Weather Review*, *108*(11), 1840–1853.

Song, X., & Zhang, G. J. (2018). The roles of convection parameterization in the formation of double ITCZ syndrome in the NCAR CESM: I. atmospheric processes. *Journal of Advances in Modeling Earth Systems*, *10*(3), 842–866.

Talib, J., Woolnough, S., Klingaman, N., & Holloway, C. (2020). The effect of atmosphere-ocean coupling on the sensitivity of the ITCZ to convective mixing. *Journal of Advances in Modeling Earth Systems*, *12*(12), e2020MS002322.

Talib, J., Woolnough, S. J., Klingaman, N. P., & Holloway, C. E. (2018). The role of the cloud radiative effect in the sensitivity of the intertropical convergence zone to convective mixing. *Journal of Climate*, *31*(17), 6821–6838.

Taylor, K. E., Stouffer, R. J., & Meehl, G. A. (2012). An overview of CMIP5 and the experiment design. *Bulletin of the American meteorological Society*, *93*(4), 485–498.

Wang, C., Zhang, L., Lee, S.-K., Wu, L., & Mechoso, C. R. (2014). A global perspective on CMIP5 climate model biases. *Nature Climate Change*, *4*(3), 201–205.

Wang, J., Kim, H., & DeFlorio, M. J. (2022). Future changes of PNA-like MJO teleconnections in CMIP6 models: Underlying mechanisms and uncertainty. *Journal of Climate*, *35*(11), 3459–3478.

Wei, H.-H., & Bordoni, S. (2018). Energetic constraints on the ITCZ position in idealized simulations with a seasonal cycle. *Journal of Advances in Modeling Earth Systems*, *10*(7), 1708–1725.

Wild, M. (2020). The global energy balance as represented in CMIP6 climate models. *Climate Dynamics*, *55*(3-4), 553–577.

Wild, M., Folini, D., Hakuba, M. Z., Schär, C., Seneviratne, S. I., Kato, S., … König-Langlo, G. (2015). The energy balance over land and oceans: an assessment based on direct observations and CMIP5 climate models. *Climate Dynamics*, *44*, 3393–3429.

Wittenberg, A. T., Rosati, A., Lau, N.-C., & Ploshay, J. J. (2006). GFDL's CM2 global coupled climate models. part iii: Tropical Pacific climate and ENSO. *Journal of Climate*, *19*(5), 698–722.

Woelfle, M., Bretherton, C., Hannay, C., & Neale, R. (2019). Evolution of the double-ITCZ bias through CESM2 development. *Journal of Advances in Modeling Earth Systems*, *11*(7), 1873–1893.

Wolding, B., Powell, S. W., Ahmed, F., Dias, J., Gehne, M., Kiladis, G., & Neelin, J. D. (2022, jul). Tropical thermodynamic–convection coupling in observations and reanalyses. *Journal of the Atmospheric Sciences*, *79*(7), 1781–1803. doi: 10.1175/jas-d-21-0256.1

Xie, S.-P., & Philander, S. G. H. (1994). A coupled ocean-atmosphere model of relevance to the itcz in the eastern pacific. *Tellus A*, *46*(4), 340–350.

Yu, L. (2019, jan). Global air–sea fluxes of heat, fresh water, and momentum: Energy budget closure and unanswered questions. *Annual Review of Marine Science*, *11*(1), 227–248. doi: 10.1146/annurev-marine-010816-060704

Yu, S., & Pritchard, M. S. (2019). A strong role for the AMOC in partitioning global energy transport and shifting ITCZ position in response to latitudinally discrete solar forcing in CESM1.2. *Journal of Climate*, *32*(8), 2207–2226.

Zeng, X., Zhao, M., & Dickinson, R. E. (1998, oct). Intercomparison of bulk aerodynamic algorithms for the computation of sea surface fluxes using TOGA COARE and TAO data. *Journal of Climate*, *11*(10), 2628–2644. doi: 10.1175/1520-0442(1998)011⟨2628:iobaaf⟩2.0.co;2

Zhang, C. (2001). Double ITCZs. *Journal of Geophysical Research: Atmospheres*, *106*(D11), 11785–11792.

Zhang, G. J., Song, X., & Wang, Y. (2019). The double itcz syndrome in GCMs: A coupled feedback problem among convection, clouds, atmospheric and ocean circulations. *Atmospheric Research*, *229*, 255–268.

Zhang, R., Wang, X., & Wang, C. (2018). On the simulations of global oceanic latent heat flux in the cmip5 multimodel ensemble. *Journal of Climate*, *31*(17), 7111–7128.

Zuidema, P., Li, Z., Hill, R. J., Bariteau, L., Rilling, B., Fairall, C., . . . Hare, J. (2012, jan). On trade wind cumulus cold pools. *Journal of the Atmospheric Sciences*, *69*(1), 258–280. doi: 10.1175/jas-d-11-0143.1

Figure 1.

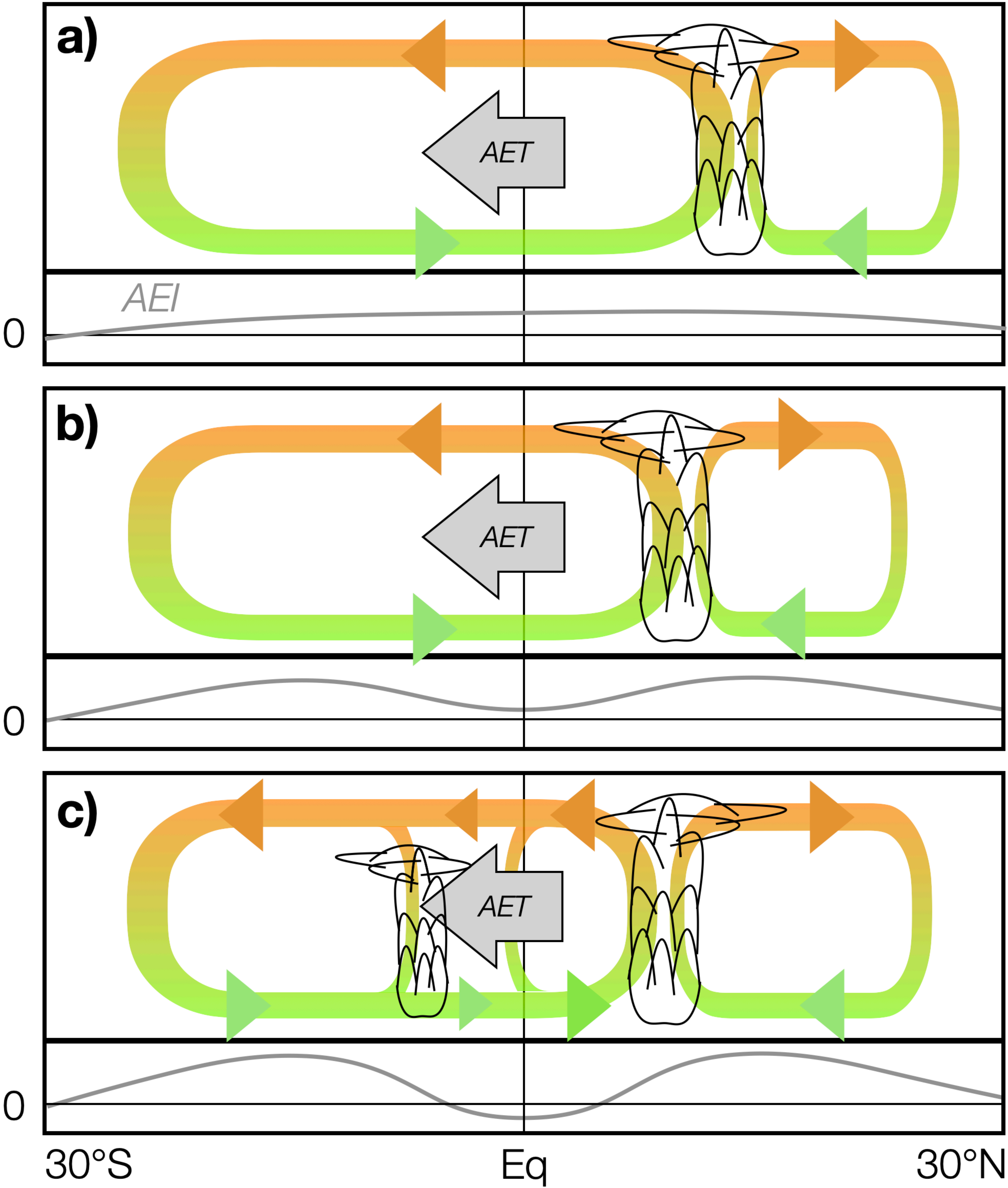
a)
AET
AEI
0
b)
AET
0
c)
AET
0
30°S
Eq
30°N

Figure 2.

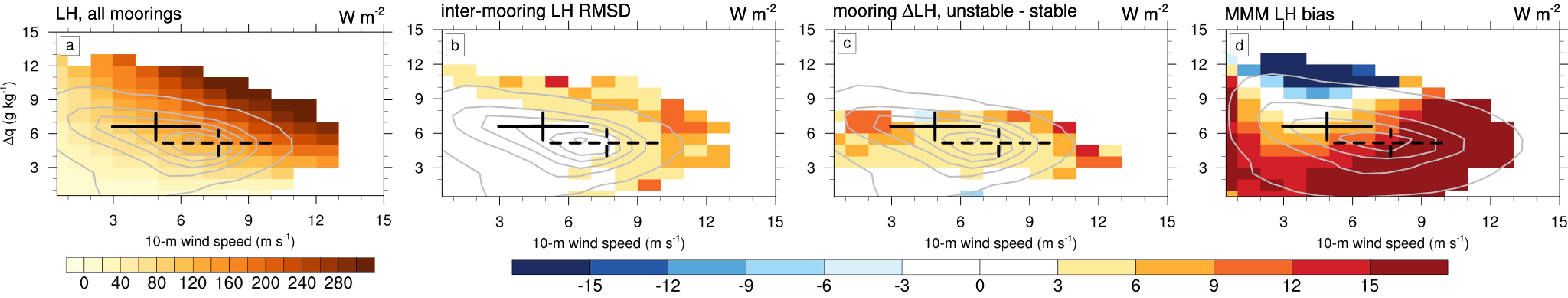
LH, all moorings
W m^{-2}
inter-mooring LH RMSD
W m^{-2}
mooring ΔLH, unstable - stable
W m^{-2}
MMM LH bias
W m^{-2}
a
b
c
d
Δq (g kg^{-1})
15
12
9
6
3
10-m wind speed (m s^{-1})
3
6
9
12
15
0
40
80
120
160
200
240
280
-15
-12
-9
-6
-3
0
3
6
9
12
15

Figure 3.

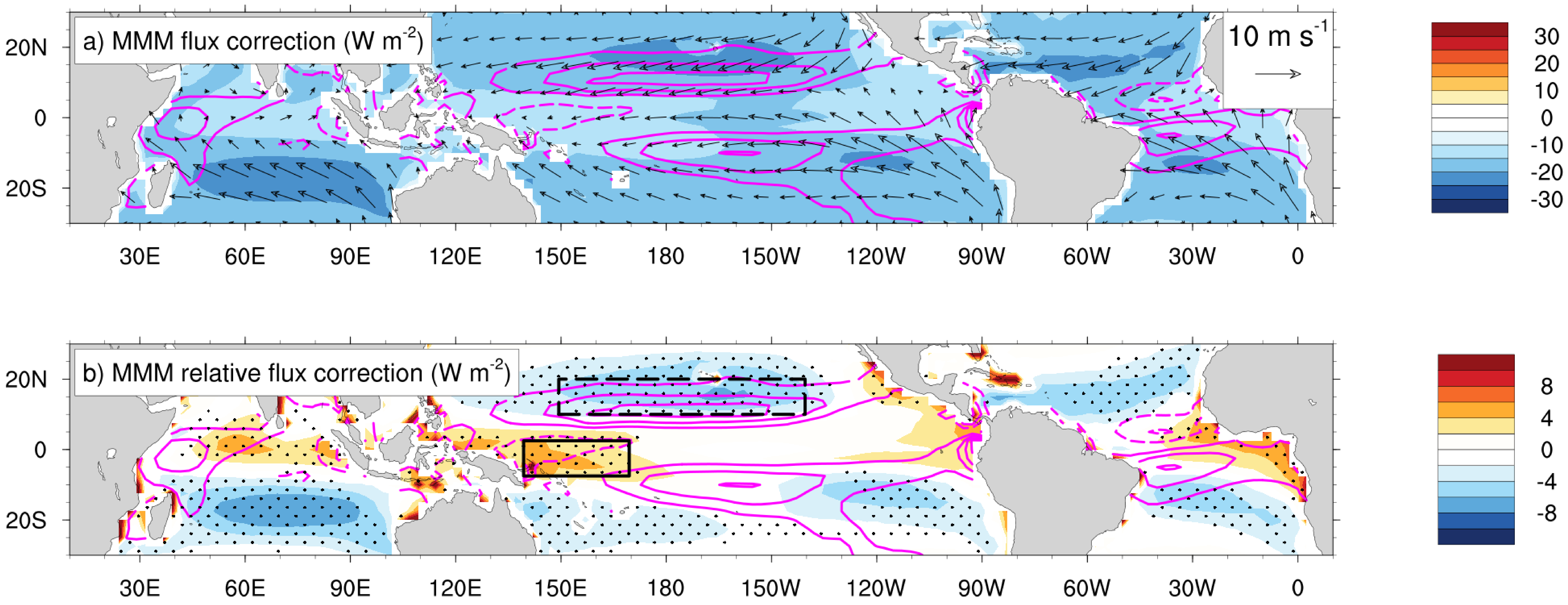
a) MMM flux correction (W m-2)
10 m s-1
20N
0
20S
30E
60E
90E
120E
150E
180
150W
120W
90W
60W
30W
0
30
20
10
0
-10
-20
-30
b) MMM relative flux correction (W m-2)
8
4
0
-4
-8

Figure 4.

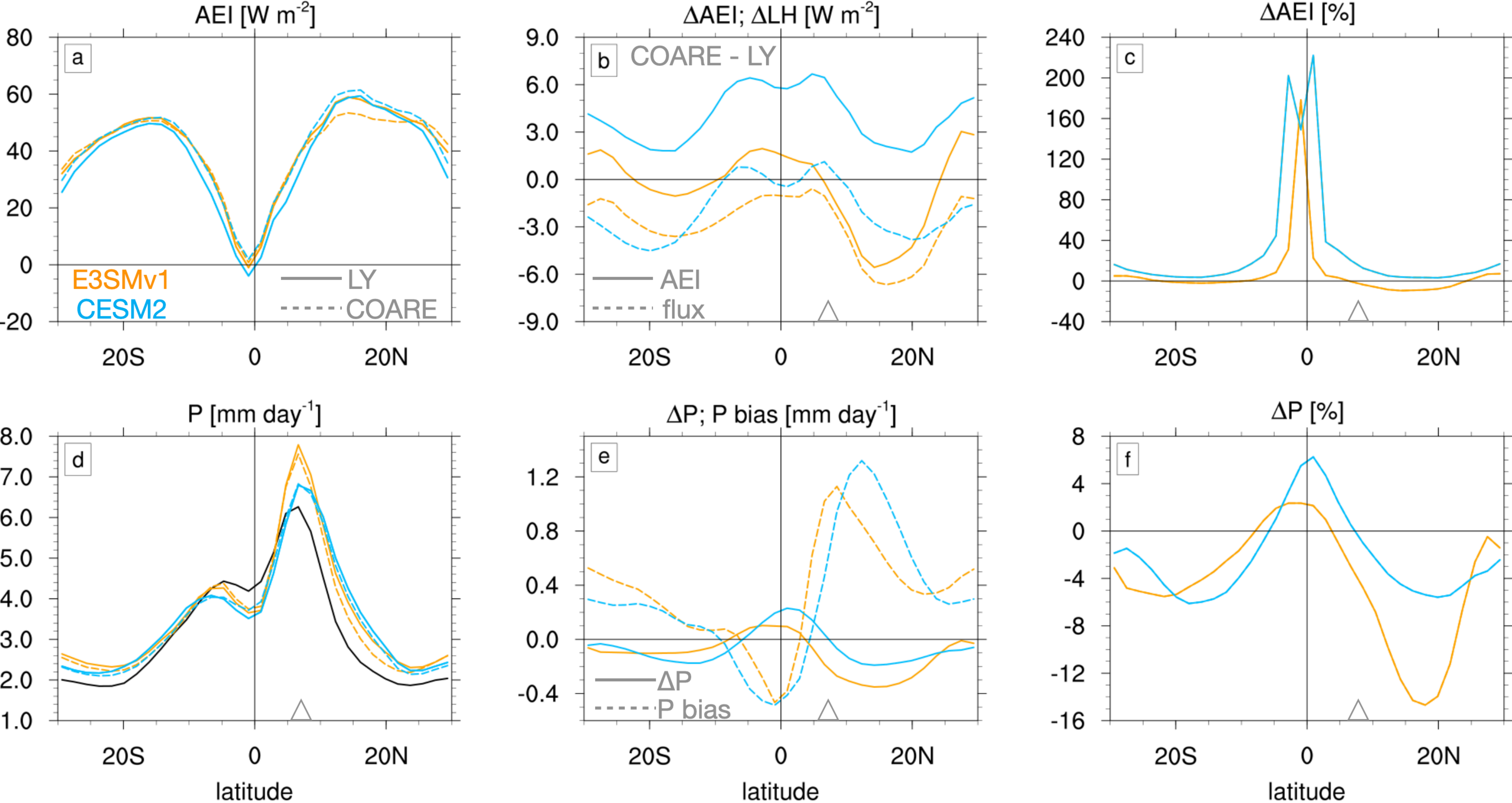
AEI [W m^{-2}]
a
E3SMv1
CESM2
LY
COARE
ΔAEI; ΔLH [W m^{-2}]
b
COARE - LY
AEI
flux
ΔAEI [%]
c
P [mm day^{-1}]
d
ΔP; P bias [mm day^{-1}]
e
ΔP
P bias
ΔP [%]
f
20S
0
20N
latitude

Figure S1.

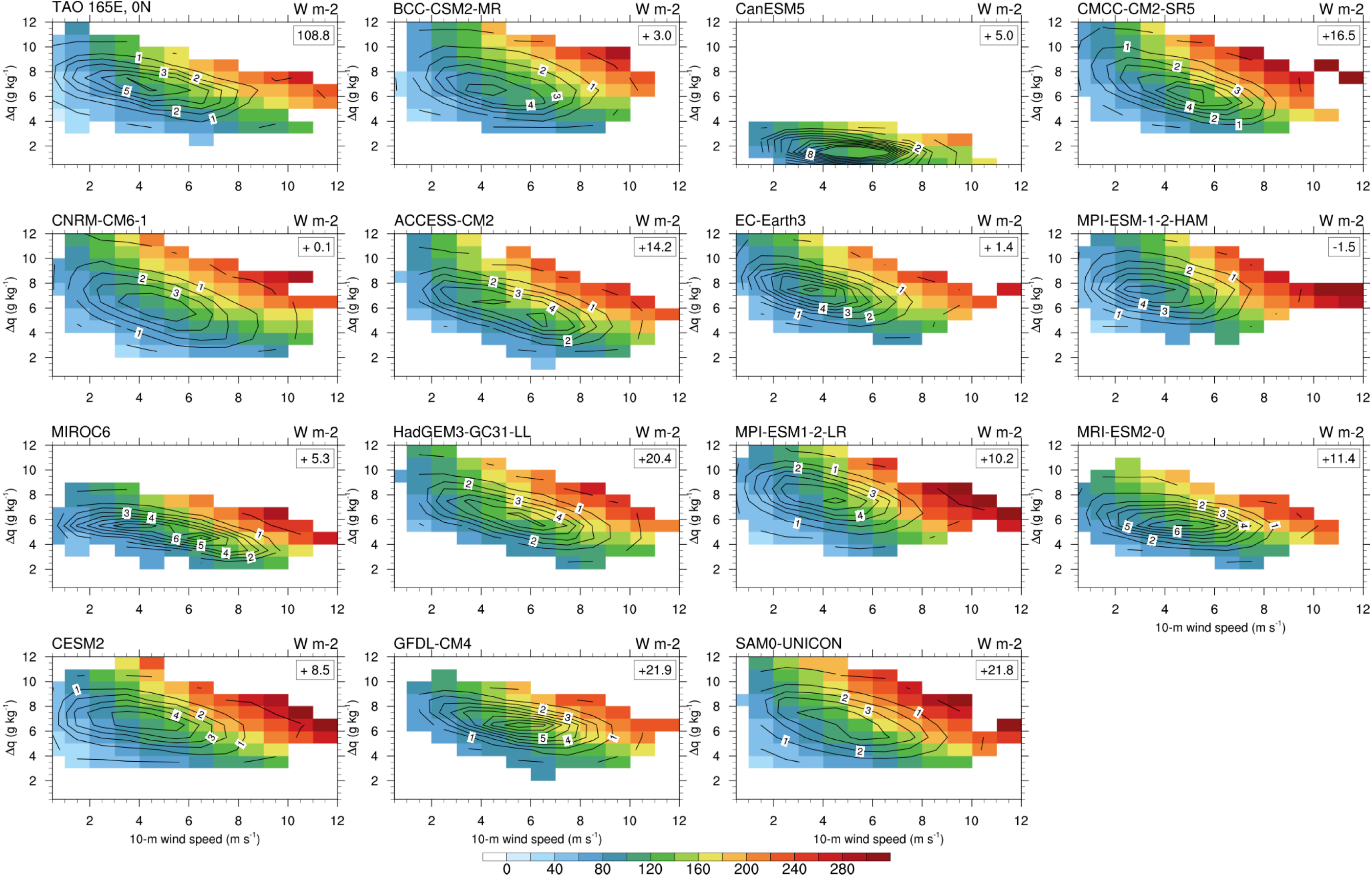
TAO 165E, 0N
W m-2
108.8
BCC-CSM2-MR
W m-2
+ 3.0
CanESM5
W m-2
+ 5.0
CMCC-CM2-SR5
W m-2
+16.5
CNRM-CM6-1
W m-2
+ 0.1
ACCESS-CM2
W m-2
+14.2
EC-Earth3
W m-2
+ 1.4
MPI-ESM-1-2-HAM
W m-2
-1.5
MIROC6
W m-2
+ 5.3
HadGEM3-GC31-LL
W m-2
+20.4
MPI-ESM1-2-LR
W m-2
+10.2
MRI-ESM2-0
W m-2
+11.4
CESM2
W m-2
+ 8.5
GFDL-CM4
W m-2
+21.9
SAM0-UNICON
W m-2
+21.8
Δq (g kg^{-1})
10-m wind speed (m s^{-1})
2
4
6
8
10
12
0
40
80
120
160
200
240
280

Figure S2.

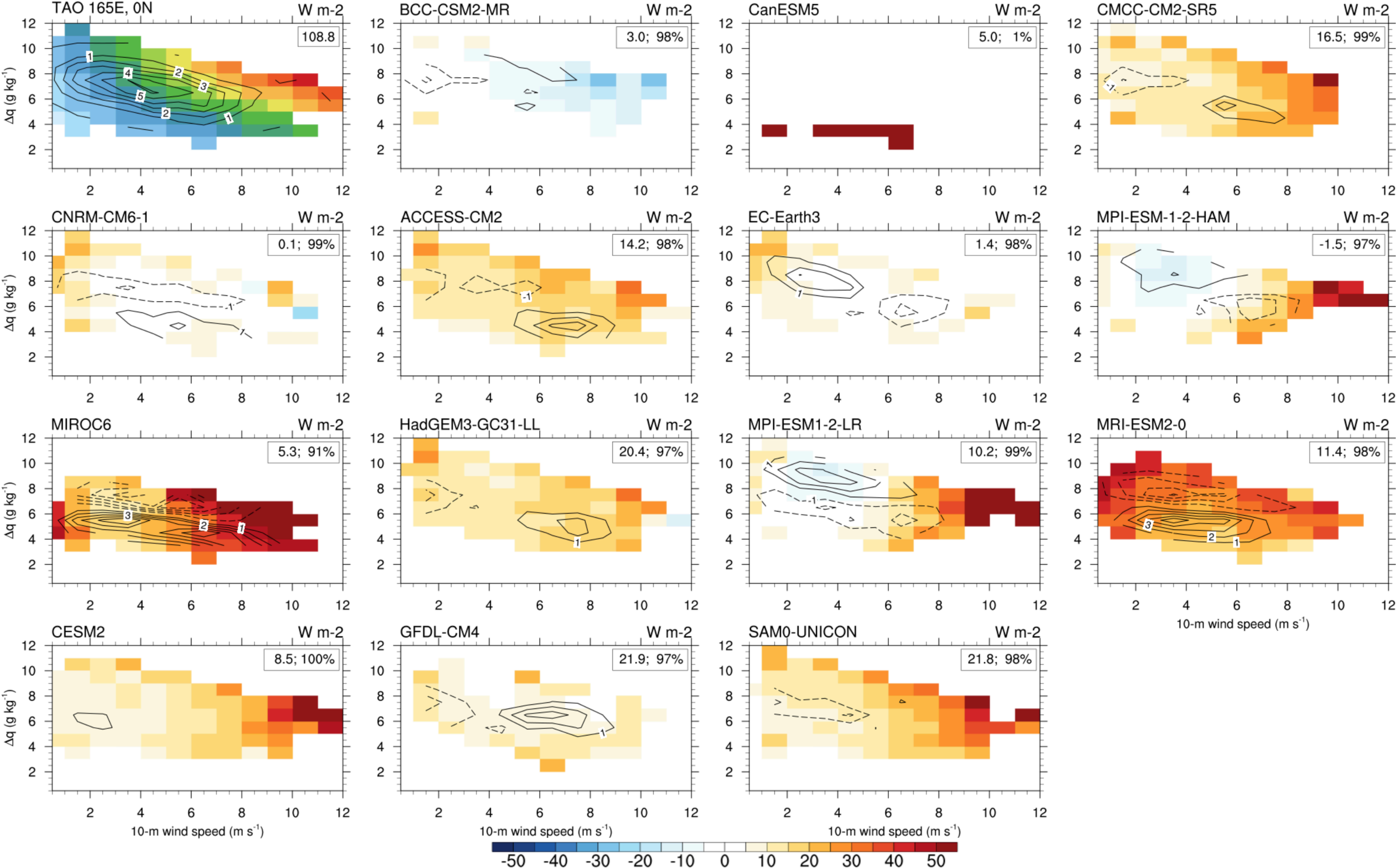
TAO 165E, 0N
W m-2
108.8
BCC-CSM2-MR
W m-2
3.0; 98%
CanESM5
W m-2
5.0; 1%
CMCC-CM2-SR5
W m-2
16.5; 99%
CNRM-CM6-1
W m-2
0.1; 99%
ACCESS-CM2
W m-2
14.2; 98%
EC-Earth3
W m-2
1.4; 98%
MPI-ESM-1-2-HAM
W m-2
-1.5; 97%
MIROC6
W m-2
5.3; 91%
HadGEM3-GC31-LL
W m-2
20.4; 97%
MPI-ESM1-2-LR
W m-2
10.2; 99%
MRI-ESM2-0
W m-2
11.4; 98%
CESM2
W m-2
8.5; 100%
GFDL-CM4
W m-2
21.9; 97%
SAM0-UNICON
W m-2
21.8; 98%
Δq (g kg^{-1})
10-m wind speed (m s^{-1})
2
4
6
8
10
12
-50
-40
-30
-20
-10
0
10
20
30
40
50

Figure S3.

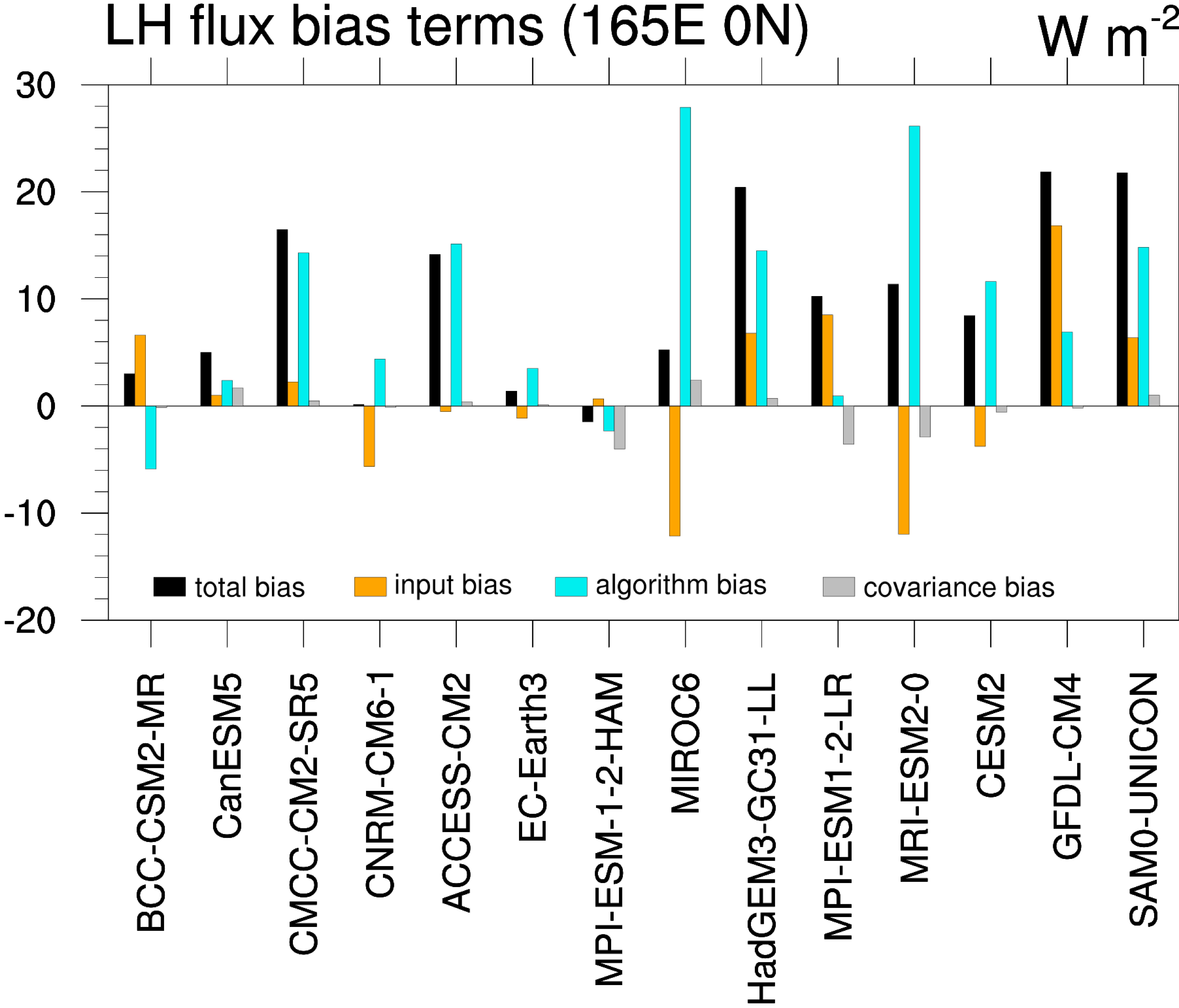
LH flux bias terms (165E 0N)
W m-2
30
20
10
0
-10
-20
total bias
input bias
algorithm bias
covariance bias
BCC-CSM2-MR
CanESM5
CMCC-CM2-SR5
CNRM-CM6-1
ACCESS-CM2
EC-Earth3
MPI-ESM-1-2-HAM
MIROC6
HadGEM3-GC31-LL
MPI-ESM1-2-LR
MRI-ESM2-0
CESM2
GFDL-CM4
SAM0-UNICON